Redox potential of the terminal quinone electron acceptor Q_B in photosystem II reveals the mechanism of electron transfer regulation

Yuki Kato[1], Ryo Nagao, and Takumi Noguchi[1]

Division of Material Science, Graduate School of Science, Nagoya University, Nagoya 464-8602, Japan

Edited by Pierre A. Joliot, Institut de Biologie Physico-Chimique, Paris, France, and approved December 4, 2015 (received for review October 12, 2015)

Photosystem II (PSII) extracts electrons from water at a Mn_4CaO_5 cluster using light energy and then transfers them to two plastoquinones, the primary quinone electron acceptor Q_A and the secondary quinone electron acceptor Q_B. This forward electron transfer is an essential process in light energy conversion. Meanwhile, backward electron transfer is also significant in photoprotection of PSII proteins. Modulation of the redox potential (E_m) gap of Q_A and Q_B mainly regulates the forward and backward electron transfers in PSII. However, the full scheme of electron transfer regulation remains unresolved due to the unknown E_m value of Q_B. Here, for the first time (to our knowledge), the E_m value of Q_B reduction was measured directly using spectroelectrochemistry in combination with light-induced Fourier transform infrared difference spectroscopy. The $E_m(Q_B^-/Q_B)$ was determined to be approximately +90 mV and was virtually unaffected by depletion of the Mn_4CaO_5 cluster. This insensitivity of $E_m(Q_B^-/Q_B)$, in combination with the known large upshift of $E_m(Q_A^-/Q_A)$, explains the mechanism of PSII photoprotection with an impaired Mn_4CaO_5 cluster, in which a large decrease in the E_m gap between Q_A and Q_B promotes rapid charge recombination via Q_A^-.

photosynthesis | spectroelectrochemistry | FTIR

In oxygenic photosynthesis in plants and cyanobacteria, photosystem II (PSII) has an important function in light-driven water oxidation, a process that leads to the generation of electrons and protons for CO_2 reduction and ATP synthesis, respectively (1–3). Photosynthetic water oxidation also produces molecular oxygen as a byproduct, which is the source of atmospheric oxygen and sustains virtually all life on Earth. PSII reactions are initiated by light-induced charge separation between a chlorophyll (Chl) dimer (P680) and a pheophytin (Pheo) electron acceptor, leading to the formation of a $P680^+Pheo^-$ radical pair (4, 5). An electron hole on $P680^+$ is transferred to a Mn_4CaO_5 cluster, the catalytic center of water oxidation, via the redox-active tyrosine, Y_Z (D1-Tyr161). At the Mn_4CaO_5 cluster, water oxidation proceeds through a cycle of five intermediates denoted S_n states (n = 0–4) (6, 7). On the electron acceptor side, the electron is transferred from $Pheo^-$ to the primary quinone electron acceptor Q_A and then to the secondary quinone electron acceptor Q_B (8, 9). Q_A and Q_B have many similarities: they consist of plastoquinone (PQ), are located symmetrically around a nonheme iron center, and interact with D2 and D1 proteins, respectively, in a similar manner (Fig. 1) (10, 11). However, they play significantly different roles in PSII (8, 9). Q_A is only singly reduced to transfer an electron to Q_B, whereas Q_B accepts one or two electrons. When Q_B is doubly reduced, the resultant Q_B^{2-} takes up two protons to form plastoquinol (PQH_2), which is then released into thylakoid membranes. Differences between Q_A and Q_B could be caused by differences in the molecular interactions of PQ with surrounding proteins in Q_A and Q_B pockets, although the detailed mechanism remains to be clarified (12, 13).

Electron transfer reactions in PSII are highly regulated by the spatial localization of redox components and their redox potentials (E_m values). Both forward and backward electron transfers are important; backward electron transfers control charge recombination in PSII, and this serves as photoprotection for PSII proteins (5, 14–17). PSII involves specific mechanisms to regulate forward and backward electron transfer reactions in response to environmental changes. For instance, in strong light, some species of cyanobacteria increase the E_m of Pheo to facilitate charge recombination. Specifically, they exchange D1 subunits originating from different *psbA* genes to change the hydrogen bond interactions of Pheo (16–20). On the other hand, it was found that impairment of the Mn_4CaO_5 cluster led to a significant increase in the E_m of Q_A by ~150 mV (21–27). This potential increase was thought to inhibit forward electron transfer to Q_B to promote direct relaxation of Q_A^- without forming triplet-state Chl, a precursor of harmful singlet oxygen (2, 5, 14, 15, 17, 23). In addition, charge recombination of Q_A^- with $P680^+$ prevents oxidative damage by high-potential $P680^+$ (5). However, the full mechanism of photoprotection by the regulation of the quinone electron acceptor E_m values remains to be resolved, because the E_m of Q_B has not been determined conclusively, and the effect of Mn_4CaO_5 cluster inactivation on it has not been examined (5).

Although the E_m of the single reduction of Q_B has been estimated to be ~80 mV higher than that of Q_A from kinetic and thermodynamic data (28–32), so far no reports have measured the E_m of Q_B directly. In contrast, the E_m of Q_A was measured extensively using chemical or electrochemical titrations and determined to be approximately −100 mV for oxygen-evolving PSII (21–27). The main reason for this difference is due to the fact that the Q_A reaction can be monitored readily by fluorescence measurement in that an increase in fluorescence indicates Q_A^- formation

Significance

In photosynthesis, photosystem II (PSII) has a function of abstracting electrons from water using light energy and transferring them to a quinone molecule. In addition to the forward electron transfer in PSII, which is essential in energy conversion, backward electron transfer is important in photoprotection of PSII proteins. Forward and backward electron transfers in PSII are regulated by the redox potential (E_m) gap of quinone electron acceptors, Q_A and Q_B. However, the regulation mechanism is still unclear because E_m of Q_B has not been determined. We directly measured E_m of Q_B using an electrochemical method in combination with Fourier transform infrared spectroscopy. Our results clearly explain the mechanism of electron transfer regulation in PSII relevant to photoprotection.

Author contributions: Y.K. and T.N. designed research; Y.K. and R.N. performed research; Y.K. and T.N. analyzed data; and Y.K. and T.N. wrote the paper.

The authors declare no conflict of interest.

This article is a PNAS Direct Submission.

[1]To whom correspondence may be addressed. Email: yuki.kato@bio.phys.nagoya-u.ac.jp or tnoguchi@bio.phys.nagoya-u.ac.jp.

This article contains supporting information online at www.pnas.org/lookup/suppl/doi:10.1073/pnas.1520211113/-/DCSupplemental.

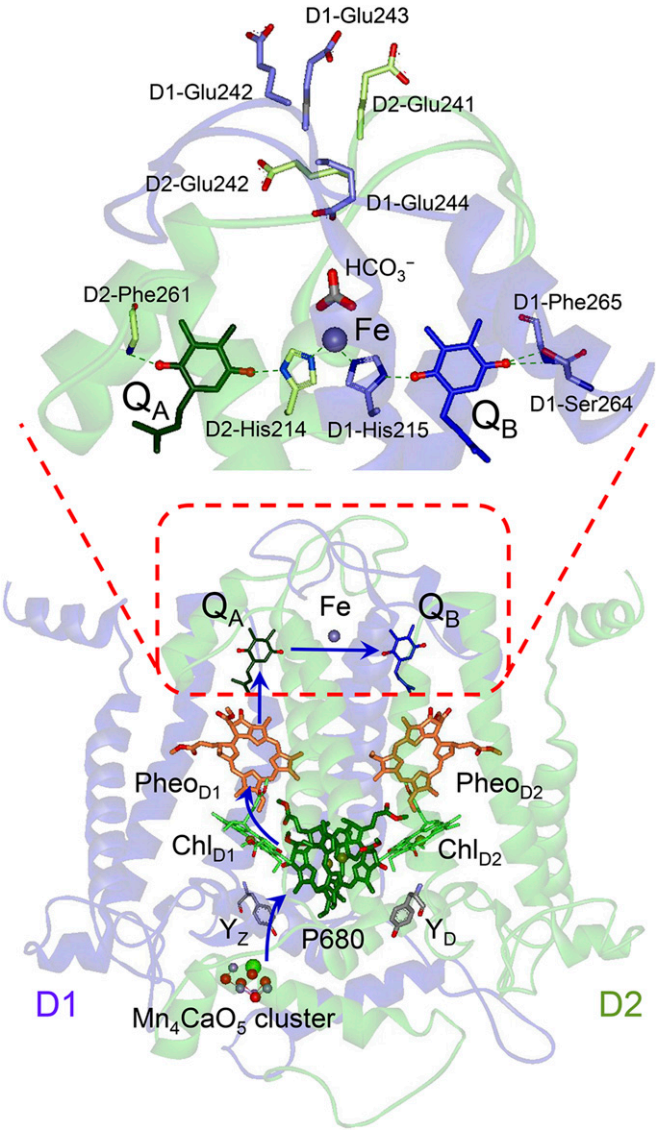

Fig. 1. Redox cofactors in PSII and the electron transfer pathway (blue arrows). For the PSII structure, the X-ray crystallographic structure at 1.9-Å resolution (Protein Data Bank ID code 3ARC) (9) was used. The electron acceptor side is expanded, showing the arrangements of Q_A, Q_B, and the nonheme iron with their molecular interactions. Nearby carboxylic groups are also shown.

(8, 33–35). However, the fluorescence method cannot be used easily to monitor Q_B reduction. Although UV-Vis absorption and electron spin resonance have also been used to monitor Q_A^- in redox titration (summarized in ref. 22), so far these methods have not been used to monitor the titration of Q_B, likely because Q_A^- and Q_B^- give similar signals (36–39). Another spectroscopic method that can be used to monitor Q_A and Q_B reactions is Fourier transform infrared (FTIR) difference spectroscopy, which detects reaction-induced changes in the molecular vibrations of a cofactor and its environment in proteins (40–45). It was previously shown that comparison of FTIR difference spectra upon Q_A^- and Q_B^- formation showed some characteristic differences in spectral features (46). In particular, bands at 1,721 and 1,745 cm^{-1}, which were assigned to ester C=O vibrations of nearby Pheo molecules affected by the reduction of Q_A and Q_B, respectively, were suggested to be good markers for discriminating between Q_A and Q_B reactions (46).

In this study, we directly measured the E_m of Q_B in PSII using spectroelectrochemistry and light-induced FTIR difference spectroscopy. The effect of Mn_4CaO_5 cluster depletion on the E_m value was also examined. Spectroelectrochemistry has been used to accurately measure the E_m values of cofactors in various redox proteins (47, 48) including redox cofactors in PSII (24, 25, 49, 50). FTIR spectroelectrochemistry, which has the additional merit of being able to provide structural information, has also been used to investigate redox reactions of biomolecules and proteins (48, 50–54). This method was recently applied to the nonheme iron center of PSII to examine the effect of Mn depletion on the E_m value and obtain structural information around the nonheme iron (50). The results in our study showed that the E_m of the first reduction of Q_B [$E_m(Q_B^-/Q_B)$] was much higher than previously estimated, and the E_m of the second reduction [$E_m(PQH_2/Q_B^-)$] was higher than the first reduction. Furthermore, we showed that Mn depletion hardly affected the E_m values of Q_B, in contrast to the large change in the E_m of Q_A (21–27). With these results, the mechanism of photoprotection of PSII when the Mn_4CaO_5 cluster is inactivated is now clearly explained.

Results

FTIR difference spectra of PSII core complexes from a thermophilic cyanobacterium *Thermosynechococcus elongatus* upon illumination of a single saturating flash were measured at a series of electrode potentials ranging from +250 to +50 mV (Fig. 2*A*). At the highest potential of +250 mV, a prominent peak was observed at 1,480 cm^{-1}, which is typical of the CO/CC stretching vibration of a Q_B^- semiquinone anion (46), whereas at the lowest potential of +50 mV, a similar peak was found at a slightly lower frequency of 1,478 cm^{-1}, which is typical of Q_A^- (55, 56). A significant change was observed in the ester C=O region (1,750–1,700 cm^{-1}): the intensity of a positive peak at 1,745 cm^{-1} decreased gradually, and a peak at 1,721 cm^{-1} increased, as the potential was lowered from +250 to +50 mV. The former and latter peaks were shown previously to belong to Q_B^-/Q_B and Q_A^-/Q_A differences, respectively, and were proposed to be good markers for discriminating between Q_B and Q_A reactions (46). Each peak was assigned to the 13^2-ester C=O vibration of the nearby Pheo ($Pheo_{D2}$ and $Pheo_{D1}$ for Q_B and Q_A, respectively; Fig. 1), which is electrostatically and/or structurally coupled to $Q_{B(A)}$ and hence affected by its photoreduction (46). The frequency difference between 1,745 and 1,721 cm^{-1} is attributed to a difference in hydrogen bond interactions of the Pheo molecules. The hydrogen bond between the 13^2-ester C=O of $Pheo_{D1}$ and D1-Tyr126 (the X-ray structure is shown in Fig. S1) provides a relatively low frequency of 1,721 cm^{-1}, whereas the corresponding residue near $Pheo_{D2}$ (D2-Phe125) does not form a hydrogen bond, and hence the C=O frequency shows a higher value at 1,745 cm^{-1}. The observed intensity changes in the 1,745 and 1,721 cm^{-1} peaks indicated that the spectrum gradually changed from Q_B^-/Q_B to Q_A^-/Q_A differences as the potential was lowered from +250 to +50 mV.

The FTIR spectra also showed a negative band at 1,401 cm^{-1} (Fig. 2*A*), which is typical of the S_2/S_1 difference and was assigned to the symmetric COO^- stretching vibrations of carboxylate groups surrounding the Mn_4CaO_5 cluster (57–59). This observation was consistent with an intact Mn_4CaO_5 cluster in the PSII sample in the spectroelectrochemical cell. It was noted that, although the intensity of this band gradually decreased as the electrode potential was lowered, it was almost fully recovered by applying a high potential of +350 mV to the sample after completion of a series of measurements from +250 to +50 mV. This observation indicated that the Mn_4CaO_5 cluster was probably reduced to lower S states such as the S_0 and S_{-1} states at lower potentials and reoxidized to the S_1 state at higher potentials.

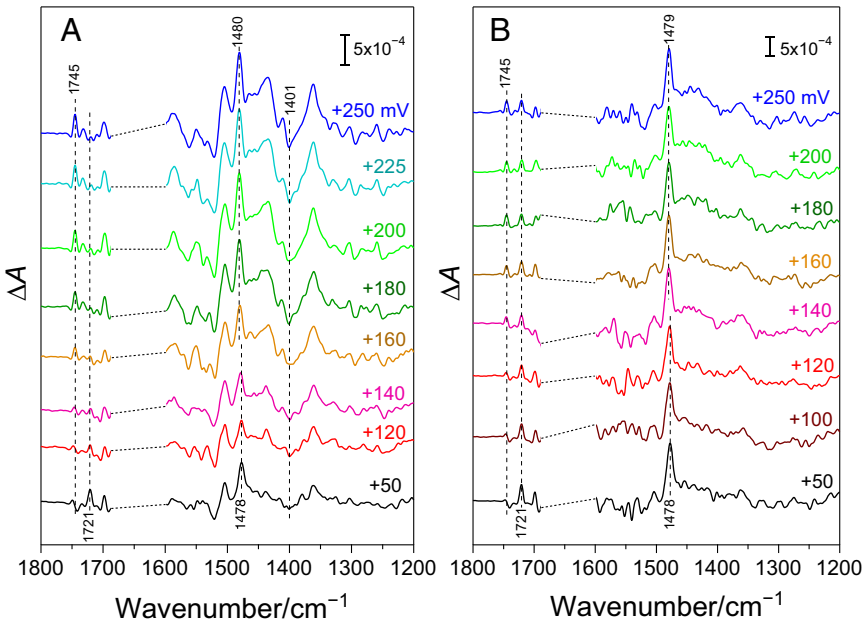

Fig. 2. Flash-induced FTIR difference spectra of the intact (*A*) and Mn-depleted (*B*) PSII core complexes from *T. elongatus* at a series of electrode potentials. A single flash from a Nd:YAG laser (532 nm, ∼7 ns) was applied to the sample equilibrated at each potential at 10 °C, and an FTIR difference spectrum was measured. The region in 1,700–1,600 cm^{-1}, which is expressed as dotted lines, is saturated by strong absorption of the amide I and water HOH bending bands.

FTIR difference spectra of Mn-depleted PSII core complexes at a series of electrode potentials (Fig. 2*B*) showed spectral features similar to those of intact PSII (Fig. 2*A*) except for the absence of a negative band at 1,401 cm^{-1} from the Mn_4CaO_5 cluster. The intensity of the peak at 1,745 cm^{-1} decreased as the potential was lowered, and almost disappeared at +100 mV. In contrast, the intensity of the 1,721 cm^{-1} peak increased at lower potentials, although it was observed even at the highest potential of +250 mV. The latter observation suggested that electron transfer from Q_A^- to Q_B was partly suppressed in Mn-depleted PSII, probably because of the unoccupied Q_B site in a fraction of centers. Note that the slightly lower frequency of the strongest CO/CC peak at 1,479 cm^{-1} at higher potentials (Fig. 2*B*) compared with the frequency of intact PSII at 1,480 cm^{-1} at similar potentials (Fig. 2*A*) can be ascribed to the contribution of the Q_A^-/Q_A signal. Indeed, a pure Q_B^-/Q_B spectrum of Mn-depleted PSII, which was obtained at +250 mV after the relaxation of Q_A^- by recording a spectrum 20 s after the flash, showed the CO/CC frequency at 1,480 cm^{-1} (Fig. S2*C*).

The reaction of Q_B was evaluated by the intensity of the 1,745 cm^{-1} peak specific to the Q_B^-/Q_B difference. To estimate the intensity of the 1,745 cm^{-1} peak accurately, the minor contribution of the Q_A^-/Q_A signal at this position (a small differential signal at 1,749/1,742 cm^{-1}) was eliminated by subtraction of the Q_A^-/Q_A difference spectrum obtained at +50 mV (Fig. 2 *A* and *B*, bottom spectrum) using a factor determined on the basis of the peak intensity at 1,721 cm^{-1}. The relative intensities of the 1,745 cm^{-1} peak (α) in the corrected spectra at a series of the potentials (Fig. 3*A*) are shown in a Nernst plot in semilogarithmic form (Fig. 3*B*). The plots for both intact and Mn-depleted PSII samples revealed a virtually linear relationship, with slopes of 30 ± 2 and 39 ± 1 mV, respectively. These slopes are close to 28 mV, the theoretical value of a two-electron reaction at 10 °C (measurement temperature), but much lower

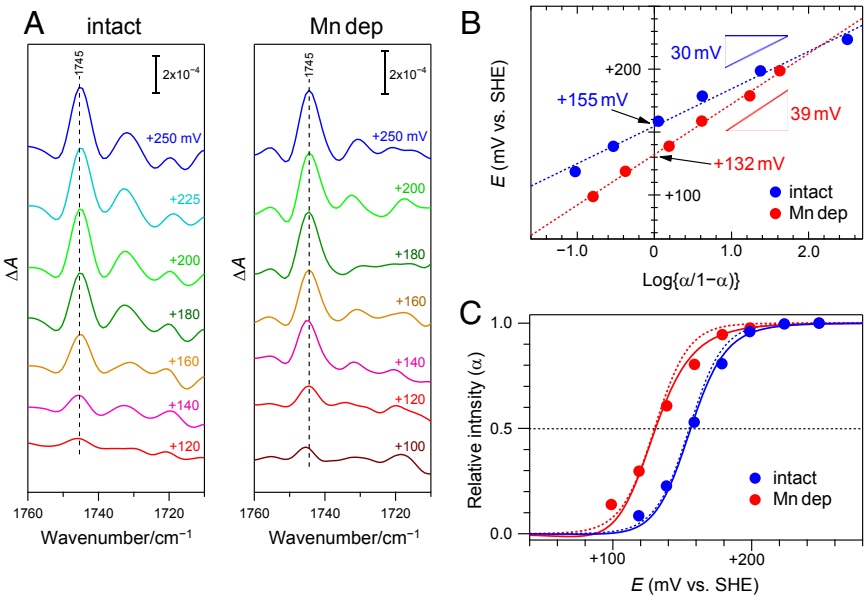

Fig. 3. (*A*) Expanded view of the 1,745 cm^{-1} band specific to Q_B^-/Q_B at a series of electrode potentials for the intact (*Left*) and Mn-depleted (*Right*) PSII core complexes. The contribution of the Q_A^-/Q_A signal (typically at 1,721 cm^{-1}) was eliminated by subtraction of the Q_A^-/Q_A difference spectrum measured at +50 mV from each spectrum. (*B*) Semilogarithmic Nernst plots of the redox reactions of Q_B in the intact (blue circles) and Mn-depleted (red circles) PSII core complexes. α indicates the intensity ratio of the 1,745 cm^{-1} peak at each electrode potential relative to the intensity at +250 mV, at which Q_B is fully oxidized. The regression lines (dashed lines) with slopes (represented by triangles) and intercepts are also shown. (*C*) Fitting of the experimental intensity ratios (α) with theoretical Nernst curves for the intact (blue lines) and Mn-depleted (red lines) PSII samples. Dashed lines reveal the theoretical curves of two-electron reactions with E_m of +155 (intact) and +132 (Mn-depleted) mV, whereas solid lines reveal the simulated curves with E_m values of the first and second reduction of Q_B as fitting parameters: $E_m(Q_B^-/Q_B)$ = +93 mV and $E_m(PQH_2/Q_B^-)$ = +213 mV for intact PSII, and $E_m(Q_B^-/Q_B)$ = +87 mV and $E_m(PQH_2/Q_B^-)$ = +157 mV for Mn-depleted PSII.

Table 1. Redox potentials of Q_B in the intact and Mn-depleted PSII core complexes from *T. elongatus* determined by FTIR spectroelectrochemistry

PSII sample	E_m^{app},* mV	$E_m(Q_B^-/Q_B)$,† mV	$E_m(PQH_2/Q_B^-)$,† mV
Intact PSII	+155	+93 ± 27	+213 ± 36
Mn-depleted PSII	+132	+87 ± 16	+157 ± 36

*Apparent E_m value obtained from the semilogarithmic Nernst plot in Fig. 3*B*.
†Values estimated by simulation using a theoretical Nernst curve with $E_m(Q_B^-/Q_B)$ and $E_m(PQH_2/Q_B^-)$ as fitting parameters.

than 56 mV, the theoretical value of a one-electron reaction. The intercepts, which indicate the apparent redox potentials (E_m^{app}) of the reaction, were estimated to be +155 ± 2 and +132 ± 1 mV for intact and Mn-depleted PSII samples, respectively. Nernst curves assuming ideal two-electron reactions with E_m values of +155 and +132 mV (Fig. 3*C*, dotted lines) largely reproduced the experimental data with slight deviations.

The fair fit with a two-electron reaction indicates that the redox potential of the second reduction of Q_B [$E_m(PQH_2/Q_B^-)$] was higher than that of the first reduction [$E_m(Q_B^-/Q_B)$], and hence Q_B was electrochemically doubly reduced to PQH_2 without forming singly reduced Q_B^- as a major component. However, an ideal two-electron curve is not realized unless $E_m(Q_B^-/Q_B)$ is at least 180 mV more negative (60) than $E_m(PQH_2/Q_B^-)$ (*SI Text* and Fig. S3). The observed spectra in Fig. 2 also support the higher $E_m(PQH_2/Q_B^-)$ than $E_m(Q_B^-/Q_B)$, because if Q_B was reduced mainly to Q_B^- at a particular potential, flash illumination would have induced a Q_B·PQH_2/Q_B^-·PQ difference spectrum providing signals with opposite intensities to the Q_B^-/Q_B spectrum, e.g., negative peaks at 1,480 and 1,745 cm^{-1}. However, such negative peaks were not observed throughout the potentials in Fig. 2. To estimate $E_m(Q_B^-/Q_B)$ and $E_m(PQH_2/Q_B^-)$ values, experimental Nernst plots were simulated using $E_m(Q_B^-/Q_B)$ and $E_m(PQH_2/Q_B^-)$ as fitting parameters (for details of the simulation, see *SI Text* and Fig. S4). In the simulation, it should be noted that the experimental relative intensity of the 1,745 cm^{-1} peak not only reflects the population of neutral Q_B but also reflects the contribution of the Q_B^- population as a negative intensity. The simulated Nernst curves (Fig. 3*C*, solid lines) provided the following data: $E_m(Q_B^-/Q_B)$ = +93 ± 27 mV and $E_m(PQH_2/Q_B^-)$ = +213 ± 36 mV with a 120-mV gap for intact PSII; $E_m(Q_B^-/Q_B)$ = +87 ± 16 mV and $E_m(PQH_2/Q_B^-)$ = +157 ± 36 mV with a 70-mV gap for Mn-depleted PSII (Table 1).

Discussion

To our knowledge, we are the first to report the successful direct measurement of E_m values of Q_B in PSII core complexes from *T. elongatus* using the spectroelectrochemical method, which uses a flash-induced FTIR signal at 1,745 cm^{-1} specific to the Q_B-to-Q_B^- change as a marker (46) (Figs. 2 and 3*A*). A Nernst plot (in semilogarithmic form) of the relative intensity of the 1,745 cm^{-1} signal suggested a two-electron reaction with a E_m^{app} of +155 mV (Fig. 3*B*, blue dashed line), suggesting that the $E_m(PQH_2/Q_B^-)$ of the second reduction of Q_B^- was higher than the $E_m(Q_B^-/Q_B)$ for the first reduction of Q_B. Further simulation of the Nernst plot estimated $E_m(Q_B^-/Q_B)$ and $E_m(PQH_2/Q_B^-)$ to be +93 ± 27 and +213 ± 36 mV, respectively, in PSII core complexes with an intact Mn_4CaO_5 cluster at pH 6.5 (Fig. 3*C* and Fig. S5, blue solid line; Table 1). The higher E_m for the second reduction compared with the first reduction, which is opposite to the general tendency of two-electron reactions, was realized by the stabilization of a doubly reduced form by the formation of neutral PQH_2 by the uptake of two protons (8, 9, 30). This has been widely seen in redox reactions of various quinone molecules in protic solvents (52, 61).

Taking into account the reported $E_m(Q_A^-/Q_A)$ value of approximately −100 mV in intact PSII (21–27), the $E_m(Q_B^-/Q_B)$ of approximately +90 mV indicates that the ΔE_m between Q_A^-/Q_A and Q_B^-/Q_B is ~190 mV (Fig. 4). This value is much larger than the ΔE_m value of ~80 mV between Q_A and Q_B previously estimated from kinetic and thermodynamic measurements using fluorescence detection (26–30). However, these measurements were performed using the herbicide 3-(3,4-dichlorophyenyl)-1,1-dimethylurea (DCMU) to accumulate Q_A^- as a reference state, without taking into consideration the influence of DCMU binding to the Q_B site on $E_m(Q_A^-/Q_A)$. It was later demonstrated that the binding of DCMU induced a positive shift of $E_m(Q_A^-/Q_A)$ by ~50 mV (62). Thus, the corrected value of ΔE_m obtained from thermodynamic measurements should be ~130 mV, which is in better agreement with, albeit still lower than, the value obtained by direct measurement in this study.

We further demonstrated that depletion of the Mn_4CaO_5 cluster induced only a small negative shift of E_m^{app} by 23 mV (Fig. 3*B*). $E_m(Q_B^-/Q_B)$ and $E_m(PQH_2/Q_B^-)$ values estimated by the simulation of the Nernst plot were +87 ± 27 and +157 ± 36 mV, respectively (Fig. 3*C*, Fig. S5, and Table 1), which indicate negative shifts of E_m by 6 and 56 mV, respectively. Taking into account the relatively large error in this simulation, this result suggests that $E_m(Q_B^-/Q_B)$ and $E_m(PQH_2/Q_B^-)$ are virtually unaffected or slightly downshifted by Mn depletion. This is in sharp contrast to the large upshift of $E_m(Q_A^-/Q_A)$ by ~150 mV upon inactivation of the Mn_4CaO_5 cluster, which was reported previously (21–27). As

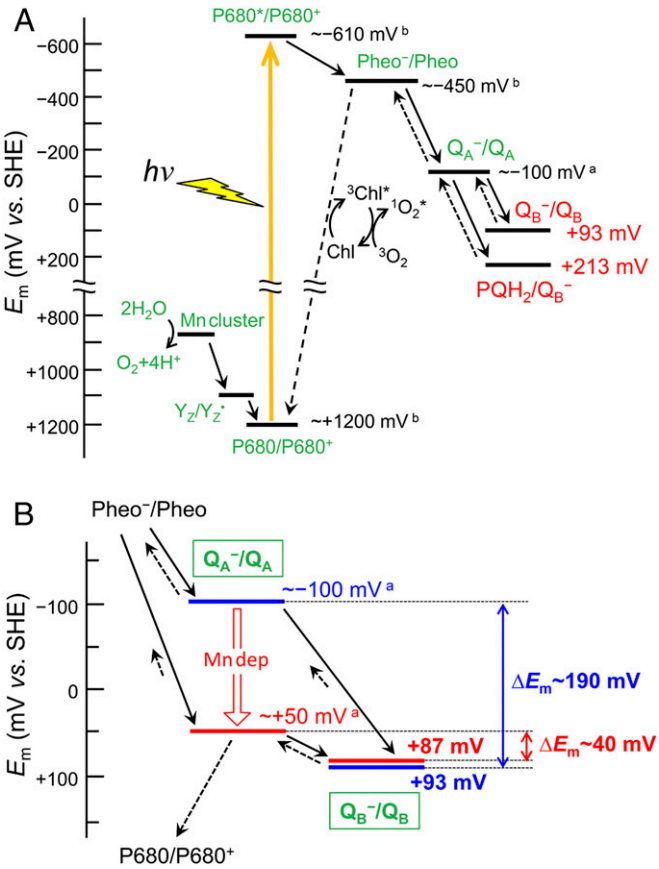

Fig. 4. (*A*) Diagram of the redox potentials of the electron transfer components in PSII. (*B*) The effect of Mn depletion on the redox potentials of single reduction of Q_A and Q_B. Solid and dashed black arrows indicate forward and backward electron transfer, respectively. The redox potential levels of intact and Mn-depleted PSII are expressed by blue and red bars, respectively, in *B*. [a]Values from refs. 19–25. [b]Values from refs. 4 and 46.

a result of the insensitivity of $E_m(Q_B^-/Q_B)$ to Mn depletion, ΔE_m between Q_A^-/Q_A and Q_B^-/Q_B largely decreased from ~190 to ~40 mV by destruction of the Mn_4CaO_5 cluster (Fig. 4*B*).

Based on these data, electron transfer regulation and hence the mechanism of PSII photoprotection are now clear (Fig. 4*B*). When the Mn_4CaO_5 cluster is impaired, $E_m(Q_A^-/Q_A)$ is significantly upshifted whereas $E_m(Q_B^-/Q_B)$ is virtually unaffected, resulting in a large ΔE_m decrease. This ΔE_m decrease promotes backward electron transfer from Q_B^- to Q_A, facilitating fast relaxation via Q_A^- by a direct charge recombination with $P680^+$, which prevents the accumulation of $P680^+$, a strong oxidant that damages PSII (5). The direct recombination of Q_A^- with $P680^+$ is further promoted by an increase in the ΔE_m between $Pheo_{D1}^-/Pheo_{D1}$ and Q_A^-/Q_A, which inhibits charge recombination via $Pheo_{D1}^-$ to generate harmful singlet oxygen via the Chl triplet state (Fig. 4*A*) (5, 14, 15, 17, 23). Thus, the regulation of E_m values of Q_A and Q_B electron acceptors upon impairment of the Mn_4CaO_5 cluster or during the process of its photoactivation protects PSII against both oxidative damage by $P680^+$ and damage by singlet oxygen.

Key elements of the mechanism of PSII photoprotection are significantly different effects of Mn_4CaO_5 cluster inactivation on the E_m values of Q_A and Q_B, i.e., largely upshifted E_m and unaffected or only slightly downshifted E_m, respectively. Q_A and Q_B are ~40 Å away from the Mn_4CaO_5 cluster, and hence the molecular mechanism of the long-range interaction between the Mn_4CaO_5 cluster and the iron–quinone complex remains poorly understood (5, 14, 21). A recent FTIR electrochemistry study (50) showed that $E_m(Fe^{2+}/Fe^{3+})$ of the nonheme iron was shifted only by +18 mV upon Mn depletion, which was much smaller than the E_m shift of Q_A. The analysis of the Fe^{2+}/Fe^{3+} FTIR difference spectra showed that Mn depletion caused some structural perturbations around the Q_B and nonheme iron sites. One change was the increase in the pK_a of a nearby Glu residue upon Mn depletion; D1-Glu244 interacting with the nonheme iron through the bicarbonate ligand was proposed to be a tentative candidate, although the possible involvement of other Glu residues located on the stromal side (Fig. 1) was not excluded. In addition, it was suggested that the hydrogen bond of one C=O of Q_B with D1-His215, which is a ligand to the nonheme iron, was strengthened, whereas the hydrogen bonds of other C=O of Q_B with the backbone NH and D1-Ser264 were weakened. However, the Q_B^-/Q_B FTIR difference spectra measured for intact and Mn-depleted PSII samples (Fig. S2) exhibited a prominent CO/CC band of Q_B^- at the same frequency of 1,480 cm^{-1}, suggesting that at least the hydrogen bond interaction of the Q_B^- was not altered significantly, which is consistent with the virtually unaffected $E_m(Q_B^-/Q_B)$. In addition, the FTIR study showed that the hydrogen bond interaction of Q_A^- was also unaffected by Mn depletion (56). Therefore, it is possible that the pK_a changes of protonatable groups including five Glu residues on the stromal side (Fig. 1) and their asymmetric distribution may have affected the E_m values of Q_A and Q_B differently; the pK_a shifts additively affected the E_m of Q_A, whereas they cancelled each other out, resulting in the unchanged E_m of Q_B. Elucidation of the route of the long-range interaction from the Mn_4CaO_5 cluster to the stromal side and the detailed mechanism of the effects on E_m values of Q_A and Q_B, which is the essence of the photoprotection of PSII, will require further investigation. In such investigations, FTIR spectroelectrochemistry combined with site-directed mutagenesis of protonatable amino acids on the stromal side will be fruitful.

Methods

The oxygen-evolving PSII core complexes were purified from cells of the *T. elongatus* 47-H strain (63), in which a $(His)_6$-tag was genetically attached to the carboxyl terminus of the CP47 subunit, using Ni^{2+}-affinity column chromatography as described previously (64). The O_2 evolution activity of PSII core complexes was 2,500–2,800 μmol $O_2 \cdot (mg\ Chl)^{-1} \cdot h^{-1}$. To deplete the Mn_4CaO_5 cluster, the PSII complexes were treated with 10 mM NH_2OH for 30 min at room temperature in the dark (65), followed by washing with Mes buffer, pH 6.5 (Buffer A: 40 mM Mes-NaOH, 5 mM NaCl, 5 mM $CaCl_2$, 0.06% *n*-dodecyl β-D-maltoside) containing 10% (wt/vol) polyethylene glycol 6000 (PEG6000) by centrifugation. After washing, the sample was suspended in Buffer A. The PSII sample (0.2 mg Chl/mL) was suspended in an electrolytic solution containing 40 mM $NaHCO_3$, 200 mM KCl, 1 M betaine, 10% (wt/vol) PEG6000, and the mixture of redox mediators in Buffer A. The redox mediators were 200 μM 1-methoxy-5-methylphanazinium methosulfate (E_m = +63 mV), 200 μM *N,N,N′,N′*-tetramethyl-*p*-phenylenediamine (E_m = +260 mV), and 4 mM potassium ferricyanide (E_m = +430 mV). For measurements of standard $S_2Q_B^-/S_1Q_B$ and S_2/S_1 difference spectra, 20 mM potassium ferricyanide was used as a sole redox mediator. The PSII sample in the electrolytic solution was centrifuged at 170,000 × *g* for 15 min, and the resulting pellet was loaded onto an optically transparent thin-layer electrode (OTTLE) cell for FTIR measurements as reported previously (50).

In the OTTLE cell, a gold mesh (60% transparent, 6-μm thickness; Precision Eforming), which was chemically modified with 4,4′-dithiodipyridine, was used as a working electrode, while a Pt black wire and a Ag/AgCl/3M KCl electrode (Cypress Systems; 66-EE009) were used as counter and reference electrodes, respectively. The sample pellet was loaded onto the gold mesh placed on a CaF_2 plate in the cell and was sandwiched with another CaF_2 plate. The assembled cell was set in a copper holder, and the sample temperature was adjusted to 10 °C by circulating cold water through the holder.

Flash-induced FTIR spectra were measured using a Bruker IFS-66/S spectrophotometer equipped with an MCT detector (D313-L/3) at 4 cm^{-1} resolution. A Q-switched Nd:YAG laser (Quanta-Ray INDI-40-10; 532 nm, ~7-ns full width at half-maximum, ~7 $mJ \cdot pulse^{-1} \cdot cm^{-2}$) was used for flash illumination. The electrode potential of the OTTLE cell was controlled using a potentiostat (Toho Technical Research; model 2020). The electrode potential was expressed against the standard hydrogen electrode (SHE). After a series of spectroelectrochemical measurements, an accurate electrode potential of the Ag/AgCl/3M KCl reference electrode (+208 mV vs. SHE) was evaluated using a standard Ag/AgCl/saturated KCl electrode (+199 mV vs. SHE), and electrode potentials were corrected. To estimate the E_m values of the Q_B redox reactions, single-beam spectra with 20 scans (10-s accumulation) were recorded before and after single-flash illumination on the PSII sample poised at different electrode potentials, and difference spectra upon illumination were calculated. At each electrode potential, the sample was stabilized for 60 min before measurement to equilibrate the redox reaction. To obtain the standard spectra of $S_2Q_B^-/S_1Q_B$ and S_2/S_1 differences with high S/N ratios, 20-scan measurements before and after flash illumination on intact PSII at electrode potentials of +350 and +470 mV, respectively, were repeated 24 times with a dark interval of 30 min, and the spectra were averaged. In the case of the S_2/S_1 difference spectrum, a 4-s delay was inserted after flash illumination to reduce the contamination of the Q_B^-/Q_B signals. For the high-quality Q_B^-/Q_B difference spectrum of Mn-depleted PSII, 20-scan measurements before and 10 s after a single flash at +250 mV were repeated 24 times with a dark interval of 1 h, and the spectra were averaged. The 20-s delay was inserted to reduce the contribution of Q_A^-, which relaxed in several seconds.

ACKNOWLEDGMENTS. This study was supported by JSPS KAKENHI [25410009 (to Y.K.), 24000018, 24107003, and 25291033 (to T.N.), and 26840091 (to R.N.)] and by Grant for Basic Science Research Projects from The Sumitomo Foundation (to Y.K.).

1. Barber J (2009) Photosynthetic energy conversion: Natural and artificial. *Chem Soc Rev* 38(1):185–196.
2. Renger G (2012) Photosynthetic water splitting: Apparatus and mechanism. *Photosynthesis: Plastid Biology, Energy Conversion and Carbon Assimilation*, eds Eaton-Rye JJ, Tripathy BC, Sharkey TD (Springer, Dordrecht, The Netherlands), pp 359–414.
3. Messinger J, Noguchi T, Yano J (2011) Photosynthetic O_2 evolution. *Molecular Solar Fuels*, eds Wydrzynski T, Hillier W (Royal Society of Chemistry, Cambridge, UK), pp 163–207.
4. Rappaport F, Diner BA (2008) Primary photochemistry and energetics leading to the oxidation of the $(Mn)_4Ca$ cluster and to the evolution of molecular oxygen in photosystem II. *Coord Chem Rev* 252(3-4):259–272.
5. Cardona T, Sedoud A, Cox N, Rutherford AW (2012) Charge separation in photosystem II: A comparative and evolutionary overview. *Biochim Biophys Acta* 1817(1):26–43.
6. Joliot P, Barbieri G, Chabaud R (1969) Model of the System II photochemical centers. *Photochem Photobiol* 10(5):309–329.
7. Kok B, Forbush B, McGloin M (1970) Cooperation of charges in photosynthetic O_2 evolution—I. A linear four step mechanism. *Photochem Photobiol* 11(6):457–475.

8. Petrouleas V, Crofts AR (2005) The quinone iron acceptor complex. *Photosystem II: The Light-Driven Water:Plastoquinone Oxidoreductase*, eds Wydrzynski T, Satoh K (Springer, Dordrecht, The Netherlands), pp 177–206.
9. Müh F, Glöckner C, Hellmich J, Zouni A (2012) Light-induced quinone reduction in photosystem II. *Biochim Biophys Acta* 1817(1):44–65.
10. Guskov A, et al. (2009) Cyanobacterial photosystem II at 2.9-Å resolution and the role of quinones, lipids, channels and chloride. *Nat Struct Mol Biol* 16(3):334–342.
11. Umena Y, Kawakami K, Shen J-R, Kamiya N (2011) Crystal structure of oxygen-evolving photosystem II at a resolution of 1.9 Å. *Nature* 473(7345):55–60.
12. Saito K, Rutherford AW, Ishikita H (2013) Mechanism of proton-coupled quinone reduction in photosystem II. *Proc Natl Acad Sci USA* 110(3):954–959.
13. Ashizawa R, Noguchi T (2014) Effects of hydrogen bonding interactions on the redox potential and molecular vibrations of plastoquinone as studied using density functional theory calculations. *Phys Chem Chem Phys* 16(24):11864–11876.
14. Rutherford AW, Osyczka A, Rappaport F (2012) Back-reactions, short-circuits, leaks and other energy wasteful reactions in biological electron transfer: Redox tuning to survive life in O_2. *FEBS Lett* 586(5):603–616.
15. Krieger-Liszkay A, Fufezan C, Trebst A (2008) Singlet oxygen production in photosystem II and related protection mechanism. *Photosynth Res* 98(1-3):551–564.
16. Vass I, Cser K (2009) Janus-faced charge recombinations in photosystem II photoinhibition. *Trends Plant Sci* 14(4):200–205.
17. Vass I (2011) Role of charge recombination processes in photodamage and photoprotection of the photosystem II complex. *Physiol Plant* 142(1):6–16.
18. Kós PB, Deák Z, Cheregi O, Vass I (2008) Differential regulation of *psbA* and *psbD* gene expression, and the role of the different D1 protein copies in the cyanobacterium *Thermosynechococcus elongatus* BP-1. *Biochim Biophys Acta* 1777(1):74–83.
19. Merry SA, et al. (1998) Modulation of quantum yield of primary radical pair formation in photosystem II by site-directed mutagenesis affecting radical cations and anions. *Biochemistry* 37(50):17439–17447.
20. Shibuya Y, et al. (2010) Hydrogen bond interactions of the pheophytin electron acceptor and its radical anion in photosystem II as revealed by Fourier transform infrared difference spectroscopy. *Biochemistry* 49(3):493–501.
21. Krieger A, Weis E (1992) Energy-dependent of chlorophyll-*a*-fluorescence: The involvement of proton-calcium exchange at photosystem 2. *Photosynthetica* 27(1-2): 89–98.
22. Krieger A, Rutherford AW, Johnson GN (1995) On the determination of redox midpoint potential of the primary quinone electron acceptor, Q_A, in photosystem II. *Biochim Biophys Acta* 1229(2):193–201.
23. Johnson GN, Rutherford AW, Krieger A (1995) A change in the midpoint potential of the quinone Q_A in photosystem II associated with photoactivation of oxygen evolution. *Biochim Biophys Acta* 1229(2):202–207.
24. Shibamoto T, Kato Y, Sugiura M, Watanabe T (2009) Redox potential of the primary plastoquinone electron acceptor Q_A in photosystem II from *Thermosynechococcus elongatus* determined by spectroelectrochemistry. *Biochemistry* 48(45):10682–10684.
25. Shibamoto T, et al. (2010) Species-dependence of the redox potential of the primary quinone electron acceptor Q_A in photosystem II verified by spectroelectrochemistry. *FEBS Lett* 584(8):1526–1530.
26. Ido K, et al. (2011) High and low potential forms of the Q_A quinone electron acceptor in photosystem II of *Thermosynechococcus elongatus* and spinach. *J Photochem Photobiol B* 104(1-2):154–157.
27. Allakhverdiev SI, et al. (2011) Redox potentials of primary electron acceptor quinone molecule $(Q_A)^-$ and conserved energetics of photosystem II in cyanobacteria with chlorophyll *a* and chlorophyll *d*. *Proc Natl Acad Sci USA* 108(19):8054–8058.
28. Diner BA (1977) Dependence of the deactivation reactions of photosystem II on the redox state of plastoquinone pool A varied under anaerobic conditions; equilibria on the acceptor side of photosystem II. *Biochim Biophys Acta* 460(2):247–258.
29. Robinson HH, Crofts AR (1983) Kinetics of the oxidation-reduction reactions of the photosystem II quinone acceptor complex, and the pathway for deactivation. *FEBS Lett* 153(1):221–226.
30. Crofts AR, Wraight CA (1983) The electrochemical domain of photosynthesis. *Biochim Biophys Acta* 726(3):149–185.
31. Minagawa J, Narusaka Y, Inoue Y, Satoh K (1999) Electron transfer between Q_A and Q_B in photosystem II is thermodynamically perturbed in phototolerant mutants of *Synechocystis* sp. PCC 6803. *Biochemistry* 38(2):770–775.
32. Rose S, et al. (2008) D1-arginine257 mutants (R257E, K, and Q) of *Chlamydomonas reinhardtii* have a lowered Q_B redox potential: Analysis of thermoluminescence and fluorescence measurements. *Photosynth Res* 98(1-3):449–468.
33. Papageorgiou GC, Govindjee (2011) Photosystem II fluorescence: Slow changes—scaling from the past. *J Photochem Photobiol B* 104(1-2):258–270.
34. Cao J, Govindjee (1990) Chlorophyll *a* fluorescence transient as an indicator of active and inactive photosystem II in thylakoid membranes. *Biochim Biophys Acta* 1015(2): 180–188.
35. Lazár D (1999) Chlorophyll *a* fluorescence induction. *Biochim Biophys Acta* 1412(1): 1–28.
36. van Gorkom HJ (1974) Identification of the reduced primary electron acceptor of photosystem II as a bound semiquinone anion. *Biochim Biophys Acta* 347(3):439–442.
37. Pulles MPJ, Van Gorkom HJ, Willemsen JG (1976) Absorbance changes due to the charge-accumulating species in system 2 of photosynthesis. *Biochim Biophys Acta* 449(3):536–540.
38. Fufezan C, Zhang C, Krieger-Liszkay A, Rutherford AW (2005) Secondary quinone in photosystem II of *Thermosynechococcus elongatus*: Semiquinone-iron EPR signals and temperature dependence of electron transfer. *Biochemistry* 44(38):12780–12789.
39. Sedoud A, et al. (2011) Semiquinone-iron complex of photosystem II: EPR signals assigned to the low-field edge of the ground state doublet of $Q_A^{\bullet-}Fe^{2+}$ and $Q_B^{\bullet-}Fe^{2+}$. *Biochemistry* 50(27):6012–6021.
40. Mäntele W (1993) Reaction-induced infrared difference spectroscopy for the study of protein function and reaction mechanisms. *Trends Biochem Sci* 18(6):197–202.
41. Noguchi T, Berthomieu C (2005) Molecular analysis by vibrational spectroscopy. *Photosystem II: The Light-Driven Water:Plastoquinone Oxidoreductase*, eds Wydrzynski T, Satoh K (Springer, Dordrecht, The Netherlands), pp 367–387.
42. Berthomieu C, Hienerwadel R (2009) Fourier transform infrared (FTIR) spectroscopy. *Photosynth Res* 101(2-3):157–170.
43. Chu H-A (2013) Fourier transform infrared difference spectroscopy for studying the molecular mechanism of photosynthetic water oxidation. *Front Plant Sci* 4:146.
44. Debus RJ (2015) FTIR studies of metal ligands, networks of hydrogen bonds, and water molecules near the active site Mn_4CaO_5 cluster in photosystem II. *Biochim Biophys Acta* 1847(1):19–34.
45. Noguchi T (2015) Fourier transform infrared difference and time-resolved infrared detection of the electron and proton transfer dynamics in photosynthetic water oxidation. *Biochim Biophys Acta* 1847(1):35–45.
46. Suzuki H, Nagasaka MA, Sugiura M, Noguchi T (2005) Fourier transform infrared spectrum of the secondary quinone electron acceptor Q_B in photosystem II. *Biochemistry* 44(34):11323–11328.
47. Dutton PL (1978) Redox potentiometry: Determination of midpoint potentials of oxidation-reduction components of biological electron-transfer systems. *Methods Enzymol* 54:411–435.
48. Melin F, Hellwig P (2013) Recent advances in the electrochemistry and spectroelectrochemistry of membrane proteins. *Biol Chem* 394(5):593–609.
49. Kato Y, Sugiura M, Oda A, Watanabe T (2009) Spectroelectrochemical determination of the redox potential of pheophytin *a*, the primary electron acceptor in photosystem II. *Proc Natl Acad Sci USA* 106(41):17365–17370.
50. Kato Y, Noguchi T (2014) Long-range interaction between the Mn_4CaO_5 cluster and the non-heme iron center in photosystem II as revealed by FTIR spectroelectrochemistry. *Biochemistry* 53(30):4914–4923.
51. Mäntele WG, Wollenweber AM, Nabedryk E, Breton J (1988) Infrared spectroelectrochemistry of bacteriochlorophylls and bacteriopheophytins: Implications for the binding of the pigments in the reaction center from photosynthetic bacteria. *Proc Natl Acad Sci USA* 85(22):8468–8472.
52. Bauscher M, Nabedryk E, Bagley K, Breton J, Mäntele W (1990) Investigation of models for photosynthetic electron acceptors: Infrared spectroelectrochemistry of ubiquinone and its anions. *FEBS Lett* 261(1):191–195.
53. Gamage RSKA, Umapathy S, McQuillan AJ (1990) OTTLE cell study of the UV-visible and FTIR spectroelectrochemistry of the radical anion and dianion of 1,4-benzoquinone in DMSO solutions. *J Electroanal Chem* 284(1):229–235.
54. Best SP (2005) Spectroelectrochemistry of hydrogenase enzymes and related compounds. *Coord Chem Rev* 249(15-16):1536–1554.
55. Berthomieu C, Nabedryk E, Mäntele W, Breton J (1990) Characterization by FTIR spectroscopy of the photoreduction of the primary quinone acceptor Q_A in photosystem II. *FEBS Lett* 269(2):363–367.
56. Takano A, Takahashi R, Suzuki H, Noguchi T (2008) Herbicide effect on the hydrogen-bonding interaction of the primary quinone electron acceptor Q_A in photosystem II as studied by Fourier transform infrared spectroscopy. *Photosynth Res* 98(1-3):159–167.
57. Noguchi T, Ono T, Inoue Y (1995) Direct detection of a carboxylate bridge between Mn and Ca^{2+} in the photosynthetic oxygen-evolving center by means of Fourier transform infrared spectroscopy. *Biochim Biophys Acta* 1228(2-3):189–200.
58. Noguchi T, Sugiura M (2003) Analysis of flash-induced FTIR difference spectra of the S-state cycle in the photosynthetic water-oxidizing complex by uniform ^{15}N and ^{13}C isotope labeling. *Biochemistry* 42(20):6035–6042.
59. Kimura Y, Mizusawa N, Ishii A, Yamanari T, Ono TA (2003) Changes of low-frequency vibrational modes induced by universal ^{15}N- and ^{13}C-isotope labeling in S_2/S_1 FTIR difference spectrum of oxygen-evolving complex. *Biochemistry* 42(45):13170–13177.
60. Bard AJ, Faulkner LR (2001) *Electrochemical Methods* (Wiley, New York), 2nd Ed.
61. Rich PR, Bendall DS (1980) The kinetics and thermodynamics of the reduction of cytochrome *c* by substituted *p*-benzoquinols in solution. *Biochim Biophys Acta* 592(3): 506–518.
62. Krieger-Liszkay A, Rutherford AW (1998) Influence of herbicide binding on the redox potential of the quinone acceptor in photosystem II: Relevance to photodamage and phytotoxicity. *Biochemistry* 37(50):17339–17344.
63. Iwai M, et al. (2010) The PsbK subunit is required for the stable assembly and stability of other small subunits in the PSII complex in the thermophilic cyanobacterium *Thermosynechococcus elongatus* BP-1. *Plant Cell Physiol* 51(4):554–560.
64. Nakamura S, Nagao R, Takahashi R, Noguchi T (2014) Fourier transform infrared detection of a polarizable proton trapped between photooxidized tyrosine Y_Z and a coupled histidine in photosystem II: Relevance to the proton transfer mechanism of water oxidation. *Biochemistry* 53(19):3131–3144.
65. Sugiura M, Inoue Y (1999) Highly purified thermo-stable oxygen-evolving photosystem II core complex from the thermophilic cyanobacterium *Synechococcus elongatus* having His-tagged CP43. *Plant Cell Physiol* 40(12):1219–1231.